Presented at BMAS ‘98: IEEE/VIUF Int. Workshop on Behavioral Modeling and Simulation, Orlando, FL, October 27-28, 1998.

NODAS 1.3 - Nodal Design Of Actuators And Sensors

Gary K. Fedder[†*] *and Qi Jing*[†]
[†]Department of Electrical and Computer Engineering and [*]The Robotics Institute
Carnegie Mellon University
Pittsburgh, PA, 15213-3890

Abstract

A circuit-level methodology for top-down hierarchical design and nodal simulation of microelectromechanical systems (MEMS) is presented. An abstract layout view is introduced as a geometrically intuitive MEMS representation that is transformed into a schematic suitable for behavioral simulation. Suspended-MEMS inertial sensors, resonant actuators and filters are designed using a small set of geometrically parameterized plate, beam, gap and anchor elements. Effects of manufacturing variations are evaluated by simply changing parameter values of the elements.
Keywords: MEMS, hierarchical modeling, nodal simulation

1: Introduction

Microelectromechanical systems (MEMS) are sensor and actuator systems made from microelectronic batch fabrication processes. Futuristic applications of MEMS, such as inertial navigation systems, high-density data storage, DNA analysis systems, and wireless distributed sensor networks, represent tantalizing opportunities for commercialization. However, successful design and manufacture of these kinds of mixed-technology systems is currently very difficult. Single-chip and hybrid versions of these systems will require integration of digital and analog electronics with tens to thousands of mechanical structures, electromechanical actuators, and various sensing elements (*e.g.,* capacitive transducers for motion sensing). One requirement for successful large-scale-system design is the formation of stable MEMS processes and access to reliable materials characterization. A second requirement is for CAD tools to support rapid top-down design of systems involving physical interactions between mechanical, electrostatic, magnetic, thermal, fluidic, and optical domains.

MEMS design needs are similar to those driving advances in analog and microwave system CAD. As is the case with pure analog design, the existence of hierarchical cell design methodologies, mixed-technology simulators, layout synthesis tools, and design-rule checking will enable MEMS engineers to build larger systems and allow them to concentrate on higher-level design issues.

The link between modeling and system simulation of microelectromechanical devices can be partitioned broadly into two different methodologies:

1) The bottom-up approach: Entire MEMS devices are modeled as a single behavioral entity and treated as “black box” components in system simulation. These macromodels may be generated through direct numerical simulation (*e.g.,* finite element analysis or boundary-element analysis) with fitting of results to appropriate analytic functions. An alternative technique employs pattern matching with arbitrary inputs to generate abstract macromodels [1]. Numerical simulation tools that are tailored for MEMS bottom-up modeling are available from several companies [2][3][4]. Generalized techniques have recently been developed for rapid modeling of micromechanical components with electrostatic actuation [5]. When using the macromodels, there is no established method for generating layout from the behavioral representation, hence the “bottom-up” designation. Physical effects can be modeled with high accuracy, however for any change in geometric parameters or topology, new models must be created, which slows design iteration.

2) The top-down approach: Hierarchical behavioral models with geometric parameters are pre-defined for a finite set of elements. For example, suspended micromechanical structures can be broken down into hierarchical building-block components. At the lowest level of the hierarchy are plate masses, beam springs, electrostatic air-gaps and anchors. These elements are analogous to resistors, capacitors and inductors in circuit design. In contrast to electrical simulation, MEMS simulation requires inclusion of geometric and layout position parameters since the micromechanical behavior is directly linked to shape of components, and, in the case of inertial sensors, is linked to absolute layout position. The primary advantages of the top-down methodology are the reusability of the parametric models and the ability to generate layout from the electromechanical components. If desirable, macromodels can be

formed *ad hoc* without loss of generality in system simulations, because of the finite number of reusable components which form the basis of a very large and useful design space. Modeling intervention during design iterations is only required when a designer insists on device topologies that cannot be constructed from parts in the library.

The top-down and bottom-up approaches are not mutually exclusive, and may be combined. The sole constraint is that component input-output relations are kept consistent.

The top-down hierarchical design representation developed at Carnegie Mellon is called NODAS, for Nodal Design of Actuators and Sensors [6]. Behavioral models of MEMS elements are currently implemented in Analogy MAST® with simulation in Saber® [7]. (MAST is a registered trademark of Analogy, Inc. Saber is a registered trademark of American Airlines, Inc., licensed to Analogy, Inc.) Similar hierarchical macromodels and nodal simulations have been developed in SPICE-like representation with simulation in MATLAB (called SUGAR) by Pister [8][9], and in MAST with simulation in Saber by Lorenz [10][11]. The main distinctions between these efforts is in the nodal representation of position and displacement, in the detailed models, and in the solvers used.

We begin with an overview of suspended surface-micromachined structures, the technology currently supported by NODAS. A discussion of the underlying models for the basic components is presented, followed by example simulations of a microresonator, a micromechanical bandpass filter, and a lateral capacitive accelerometer.

2: Surface Micromechanics

A relatively mature manufacturing technology in MEMS is surface micromachining, as exemplified by the recent success of commercial accelerometers for automotive airbag deployment [12][13] and digital mirror displays for high-fidelity video projection [14]. Successful design and manufacturing of these devices required years of effort, partly due to a lack of adequate system-level MEMS design tools.

The availability of accumulated design expertise, stable fabrication services, and electromechanical CAD modeling tools has made the suspended-MEMS technology a suitable candidate for development of circuit-level design tools for MEMS. Our discussion of structured design will be restricted to suspended MEMS, however the concepts apply to other technologies, such as high-aspect-ratio silicon structures.

The polysilicon (thin-film polycrystalline silicon) surface-micromachining process was originally developed in parallel by researchers at U. C. Berkeley, MIT, and Bell Labs, and is commercially available in the Multi-User MEMS Process service (MUMPs) from MCNC [15]. In this process, the micromechanical components are made entirely from a homogeneous, conducting, 2 μm-thick polysilicon film. The movable microstructure is fixed to the substrate through anchor points, which also act as electrical vias. The 2 μm air-gap separation, g, between the structures and the substrate is formed by wet etching a sacrificial oxide film under the structure.

The microresonator shown in Figure 1 is a popular polysilicon MEMS device, first described and analyzed by Tang [16]. It is used in high-quality-factor resonator oscillators and bandpass filters [17], as a resonant actuator for stepper motor drives [18], and as a mechanical characterization test structure to measure Young's modulus of thin films.

The central shuttle mass suspended by two folded-beam flexures forms a mechanical mass-spring-damper system. Viscous air damping is the dominant dissipation mechanism at atmospheric pressure. The beams in the folded flexure expand outward to relieve residual stress in the film, and inhibit buckling. The resonator is driven in the preferred (x) direction by electrostatic comb-finger actuators that are symmetrically placed on the sides of the shuttle. The suspension is designed to be compliant in the x direction of motion and to be stiff in the orthogonal direction (y) to keep the comb fingers aligned.

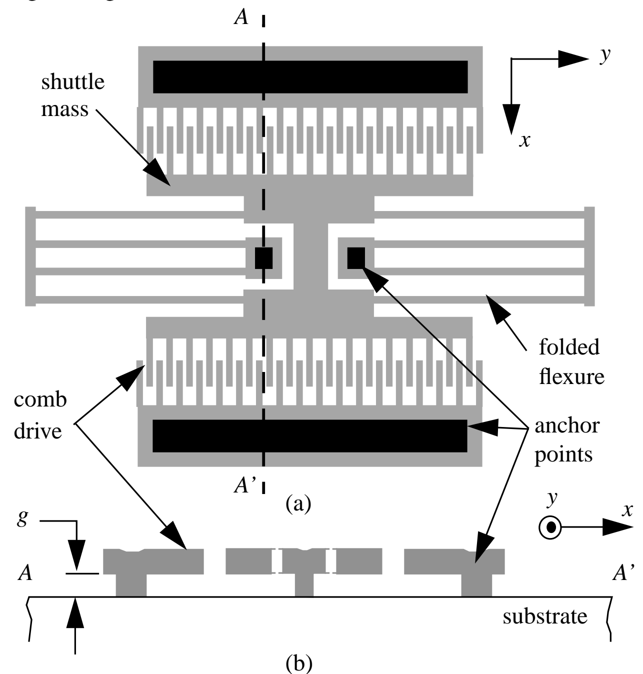

FIGURE 1. A folded-flexure comb-drive microresonator fabricated in a polysilicon surface microstructural process. (a) Layout. (b) Cross-section *A-A'*.

3: Circuit-Level Design Methodology

All suspended structures respond to inertial forces, so any methodology should include these effects. Inertial sensors respond to acceleration and rotation with respect to a fixed frame of reference, whereas the transducers detect displacement relative to the package, or chip, frame of reference. On-chip actuation is also relative to the chip frame of reference. The relationship between the two frames is shown in Figure 2. The specification of rigid-body position of each element in the fixed frame is necessary for calculation of rotational inertial forces.

In our prior work on NODAS [19][6][20], a methodology was developed for top-down MEMS design using an abstracted layout representation, illustrated in Figure 3 for a simple cantilever beam. In-plane displacements (δx, δy, $\delta\theta$) were defined as across variables, and forces and torques (F_x, F_y, M_θ) acting on the element were through variables. Rigid-body position (X, Y, Θ) was included as a distinct set of across variables, so that the time-varying translation and rotation of the chip was propagated to all of the elements. The through variables at the layout nodes had no physical meaning.

Sign conventions can be stated rather simply and are essential for physically interpreting the simulation results. The δx and δy across variables are positive in the positive-axis directions and $\delta\theta$ is positive in a counterclockwise rotation (right-hand rule) around the positive z axis. Through variables going *into* a node are interpreted as providing force in the positive-axis direction or providing torque in a counterclockwise rotation around the positive z axis. The through variable sign convention is illustrated in Figure 3 at port b. (Here, "port" is used to denote the 7 nodes associated with a physical point on an element.)

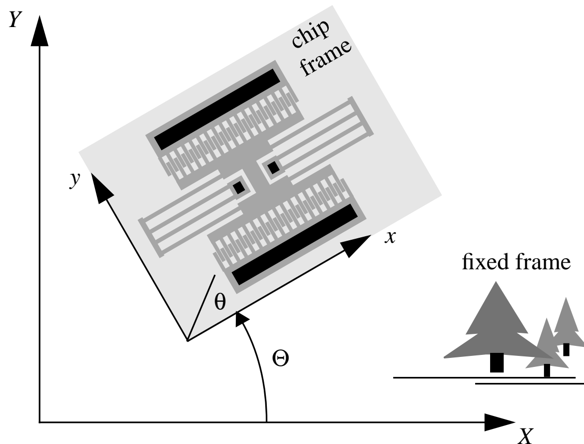

FIGURE 2. Fixed frame of reference *(X, Y, Θ)* and chip frame of reference *(x, y, θ)*.

Including rigid-body position in the nodal analysis allows users to build new designs without manually calculating the layout position of each element. Instead, the simulator calculates the layout position through the dc analysis. However, the initial approach in NODAS has two major drawbacks. First, the extra position nodes enlarge the solution matrix and slow down the simulation. Second, representing steady-state acceleration (*e.g.,* gravity) in terms of position produces large nodal position values and leads to an ill-conditioned specification of the problem after long transient simulation times.

We have created new MEMS element models, illustrated in Figure 4, that decouple the calculation of layout

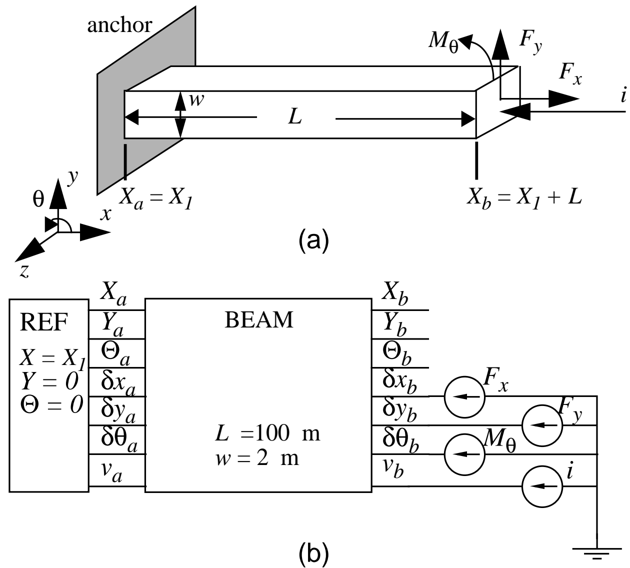

FIGURE 3. Previous nodal representation of a simple cantilever beam with in-plane layout position *(X, Y, Θ)* and displacements *(x, y, θ)*. (a) Physical view. (b) Schematic view.

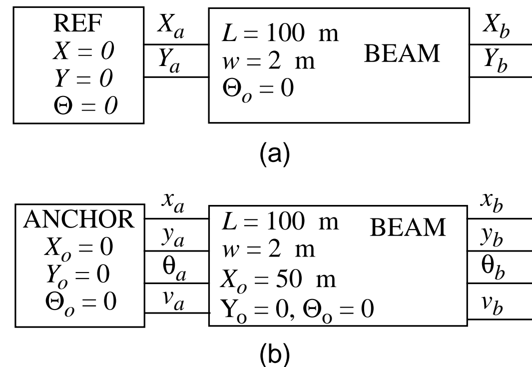

FIGURE 4. Revised representation of a simple cantilever beam. (a) Abstract layout representation using geometric models. (b) Schematic functional representation using behavioral models to determine displacement.

position from the behavioral simulation. The user creates a schematic using the abstracted layout components in Figure 4(a). The results of the dc simulation are the layout positions of the elements, which are used to generate a new behavioral schematic having layout position automatically specified as a component parameter. The 50% reduction of mechanical nodes from our prior models provides more rapid simulation. A similar formulation has been developed for microgyroscope behavioral models by Lorenz [10] in which the layout position of each element is embedded as a static parameter specified by the user. However, the abstract layout input representation in NODAS eliminates layout position entry errors by the user.

Behavioral models for the mechanical elements are based on theory of structural analysis [21] and are given in explicit detail in [6]. Currently, we have modeled four basic elements: the straight beam, rigid plate, electrostatic comb-finger actuator, and anchor. Forces are calculated in the local frame of reference of each instance of an element and then transformed into the chip frame of reference for addition to the through variables using a static rotational matrix, $[T]$. The anchor model sets displacement to zero.

A straight beam is modeled as a linear spring element with a stiffness matrix, $[k]$, found by direct solution of the beam bending equation. Inertial force is modeled with a mass matrix, $[m]$, found by assuming static shape functions which link acceleration at the nodes to the distributed force along the beam. Damping is modeled as Couette air damping with damping matrix, $[B]$. The force variables in the local frame are

$$\left[F_{beam}\right] = \left[m\right]\left[\ddot{x}\right] + \left[B\right]\left[\dot{x}\right] + \left[k\right]\left[x\right] \tag{1}$$

where $[x] = [T]^{-1}[\delta x_a\ \delta y_a\ \delta\theta_a\ \delta x_b\ \delta y_b\ \delta\theta_b]$ are the displacements at beam's nodes a and b. The through variables for the forces and moments in the chip frame are given by $[F_{x,a}\ F_{y,a}\ M_a\ F_{x,b}\ F_{y,b}\ M_b] = [T][F_{beam}]$. In contrast to current through electrical elements, the through variables for forces and moments at external node a are not necessarily the same value as corresponding values at node b.

Plates are treated as rigid bodies, so the inertial mass for translational motion is simply equal to the material density times the plate volume. Damping is modeled as Couette air damping, which is proportional to the area of the plate [22]. The plate force variables are

$$\left[F_{plate}\right] = \left[m_p\right]\left[\ddot{x}\right] + \left[B_p\right]\left[\dot{x}\right] \tag{2}$$

where $[x] = [\delta x_m\ \delta y_m\ \delta\theta_m]$ is the displacement at the center of mass of the plate and $[F_{plate}] = [F_{x,m}\ F_{y,m}\ M_m]$ are the corresponding rigid-body forces and moments.

Lateral electrostatic actuator models are based on nonlinear analytic equations for air-gap capacitance across the actuator electrodes. A first-order model assumes a parallel-plate sidewall capacitance,

$$C = \frac{\varepsilon A_{eff}}{g(\delta x, \delta y, \delta\theta)} \tag{3}$$

where A_{eff} is the effective electrode area including fringing field effects, and g is the air gap expressed as a function of electrode displacement. The electrostatic force between the two electrodes is

$$\left[F_e\right] = \frac{1}{2}\left[\frac{\partial C}{\partial x_i}\right]v^2 \tag{4}$$

where x_i are the individual terms in $[x]$ at the actuator's nodes a and b. The matrix terms are calculated in the actuator's local frame. The actuator model also includes rigid-body mass and damping terms, similar to the plate model.

4: Simulation Results

4.1: Microresonator

The abstract layout view of the folded-flexure resonator is shown in Figure 5. The folded-flexure suspension is partitioned into 14 beam elements, and the central shuttle mass is partitioned into five plate elements. The comb-finger actuators are modeled as single elements. Each element serves both an electrical and mechanical role. A voltage source drives the lower actuator, while a dc bias voltage, V_{dc}, is applied to the moving structure. Displacement current ($i = V_{dc}\ dC/dt$) through the time-varying capacitance of the upper comb drive is sensed with a transresistance amplifier.

The beam and plate models are verified by comparing mechanical simulation with finite-element results using ABAQUS [23]. Static analysis of the shuttle displacement as a function of comb-drive voltage, shown in Figure 6 is performed through dc transfer-function analysis. The V^2 nonlinearity of the force-displacement relation is readily apparent. The ac response of the resonator to a sinusoidal comb-drive voltage with a dc bias on the shuttle is given in Figure 7. The mechanical simulation results are within 1% of values generated using finite-element analysis.

4.2: Micromechanical Filter

An abstracted layout view of the micromechanical filter introduced by Nguyen [17] is shown in Figure 8. Three folded-flexure microresonators, each having a slightly different resonant frequency, are mechanically coupled together

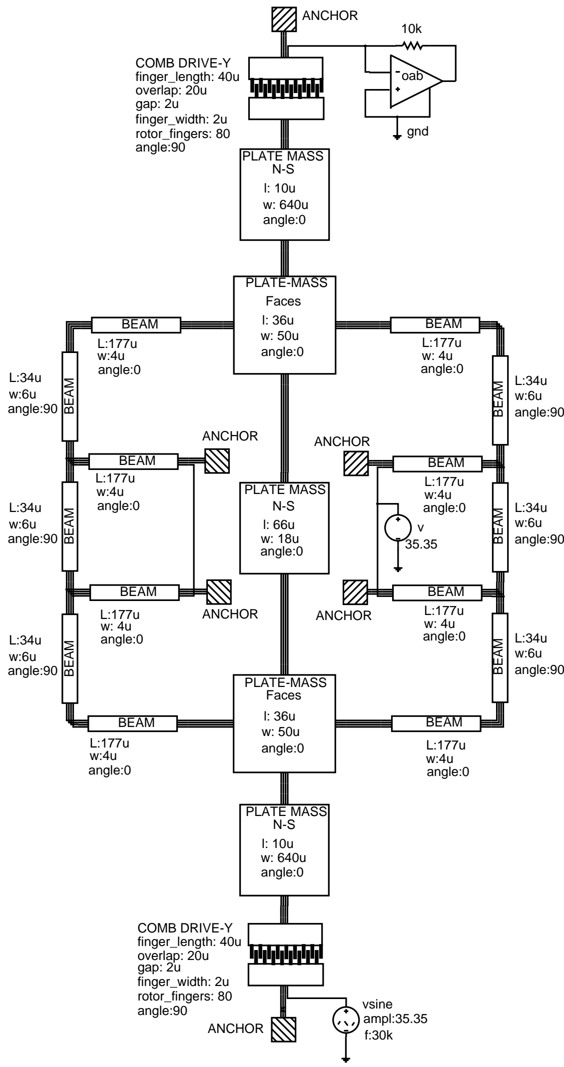

FIGURE 5. Abstract layout view in SaberSketch of the folded-flexure comb-drive microresonator shown in Figure 4. Parameter values are listed next to the element symbol.

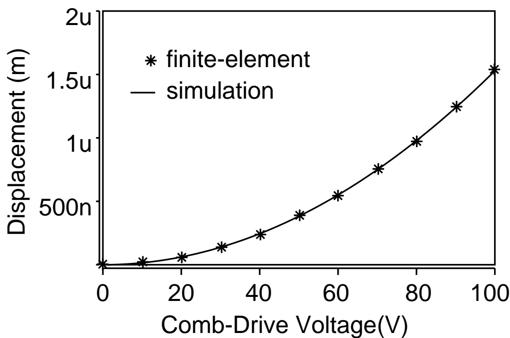

FIGURE 6. Static analysis of microresonator displacement as a function of applied voltage. Points derived from finite-element static and modal analysis are plotted for comparison.

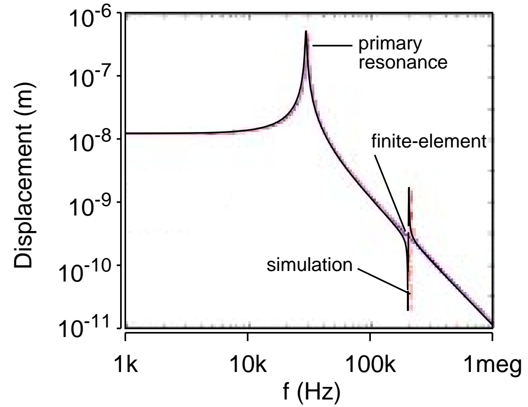

FIGURE 7. Frequency response of the micro-resonator displacement. The second-order response derived from finite-element static and modal analysis is plotted for comparison.

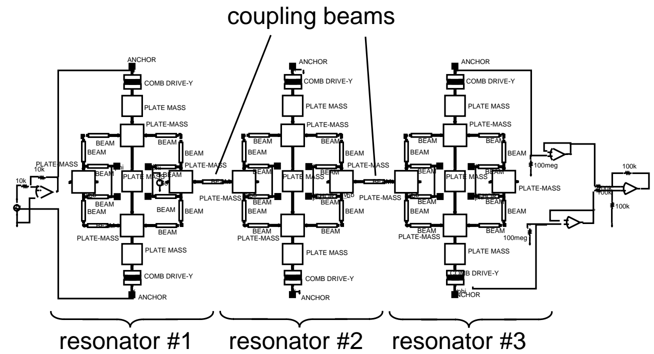

FIGURE 8. Abstract layout view of a micro-mechanical bandpass filter.

with beams connecting neighboring trusses. By choosing the size of the coupling beams appropriately, a narrow-band bandpass filter can be implemented. The filter is a good example of a hierarchically designed MEMS. The schematic was rapidly assembled by copying the pre-assembled resonator model three times and then adding the coupling beams. The sharp passband, shown in the ac analysis results in Figure 9, compares very well qualitatively with Nguyen's SPICE model simulation. The two peaks in the passband are from deviation in the ideal size of the coupling beams.

4.3: Lateral Crab-Leg Accelerometer

The accelerometer shown in Figure 10, is a plate mass connected to a crab-leg suspension. Each "crab leg" is created by joining two beams at 90°. The crab-leg accelerometer is similar to the microresonator in that both are suspended plate masses with two comb-finger capacitors attached to opposing sides of the plate. For the accelerome-

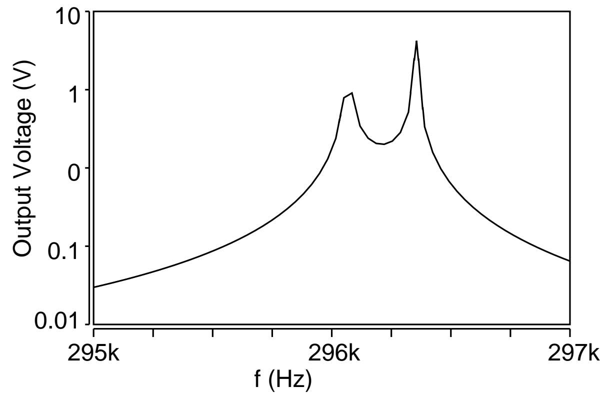

FIGURE 9. Micromechanical filter simulation. The dip in the passband is from tuning mismatch in the coupling beams.

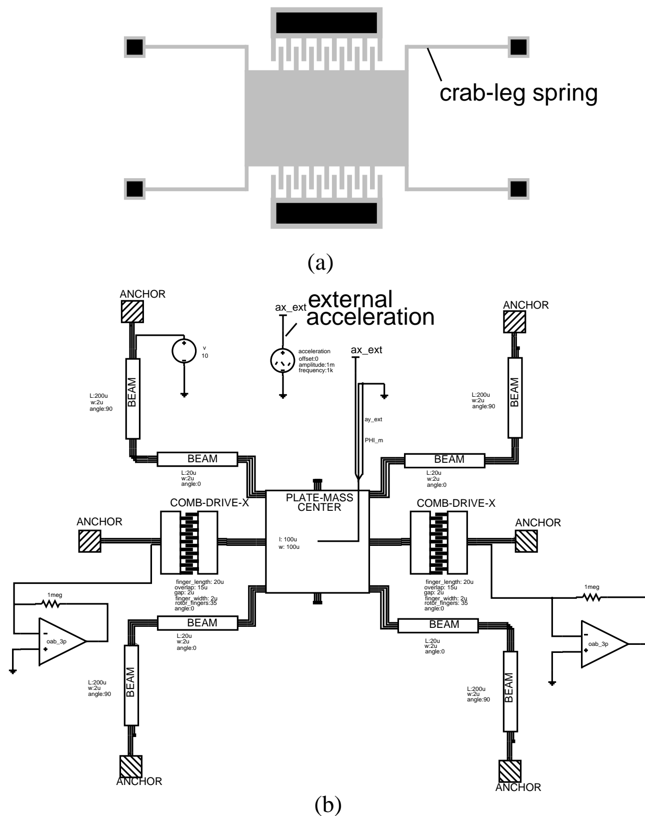

FIGURE 10. Design of a crab-leg accelerometer. (a) Simplified layout. (b) Abstract layout view (rotated by 90˚) with an external acceleration source.

ter, both comb-finger capacitors are connected to transresistance amplifiers to detect current due to inertial motion of the center plate. A dc voltage is impressed on the plate to provide the charge bias. The output voltage represents the first derivative of the acceleration, since the displacement

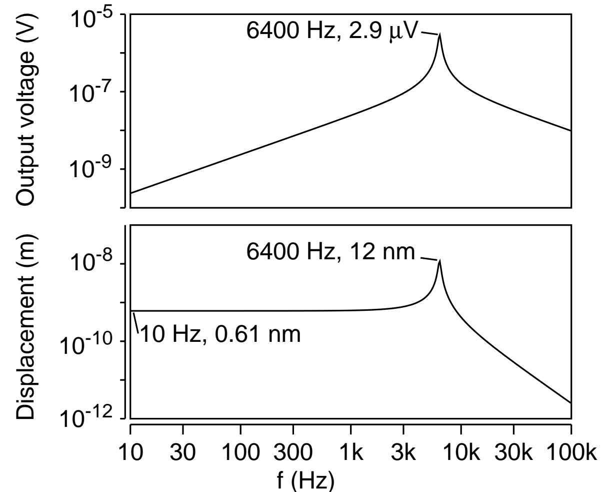

FIGURE 11. Shaker test of the accelerometer using ac simulation. The external acceleration amplitude is 1 m/s^2. Points derived from finite-element static and modal analysis are plotted for comparison.

current through the air-gap capacitor is proportional to the velocity of the proof mass, not to the displacement.

A mechanical shaker test jig is implemented by attaching an ac source to the external acceleration input. Results are shown in Figure 11. The accelerometer frequency response is within 1% of values generated using finite-element simulation. The output voltage amplitude increases with frequency for excitation frequencies less than the mechanical resonance, as expected for differentiation of the plate position. The elimination of the rigid-body position nodes in the new models greatly speeds up simulations that involve external acceleration. Simulation times are about 60% faster for ac analysis and 70% faster for transient analysis. The ac simulation was completed in 9 seconds on an 200 MHz Ultrasparc 2 workstation with 256 MB RAM.

The transient response to a 4 ms pulse in external acceleration is shown in Figure 12. The response is underdamped and the voltage only responds to changes in acceleration, as expected.

One important issue with accelerometer design is the determination of sensitivity to manufacturing variations. In the accelerometer schematic, geometric parameter values of beams and plates may be changed to determine their effect on output sensitivity and cross-axis sensitivity. Figure 13 shows the frequency response of the cross-axis acceleration for a beam variation of 1% and 10%. Small changes on the order of 10% on width of one of the four crab-leg beams causes an increase in cross-axis sensitivity to 0.01% of the direct-axis signal.

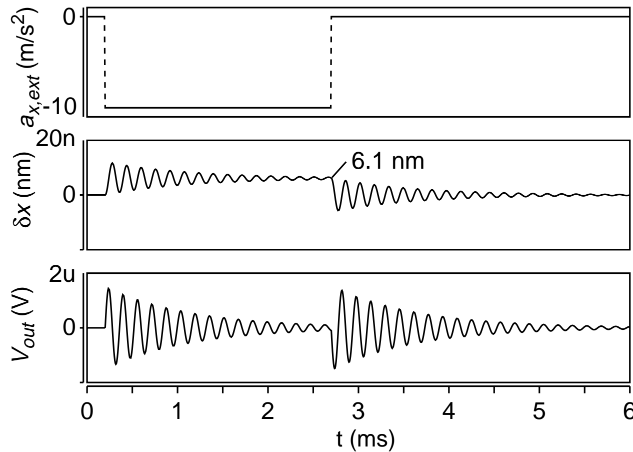

FIGURE 12. Transient response of displacement and output voltage to a pulse in external acceleration.

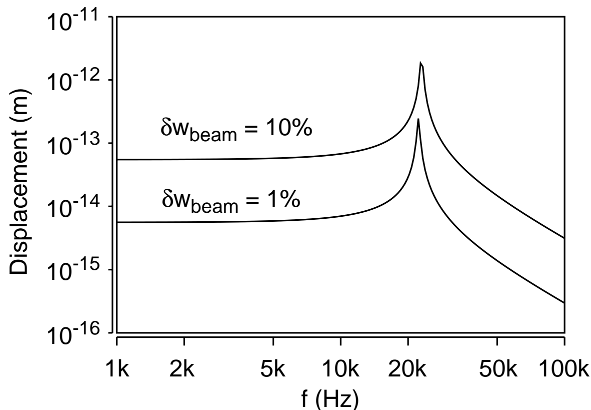

FIGURE 13. Response to cross-axis acceleration of amplitude 1 m/s^2 for different manufacturing variations. The width of one of the beams is reduced by 1%, then 10%.

5: Conclusions

Structured design methods for suspended MEMS promise to shorten the development cycle to days, and enable design of more complex systems comprised of hundreds to thousands of micromechanical elements. Identification of reusable hierarchical representations of MEMS components is a critical first step in advancing toward a structured design methodology and in leveraging existing CAD tools.

It has been shown that top-down representations for MEMS design using a hierarchical set of MEM components can be interconnected in a general way to create more complicated components and systems. Coupling the methodology with existing schematic capture tools that are compatible with electrical circuit analysis enables quick and efficient MEMS design. A key feature is the abstract layout view, which provides an intuitive interface for the designer, and provides a path for direct generation of layout from schematic.

MEMS elements with geometrically parameterized models are very useful in evaluating the influence of manufacturing variations. When using the top-down design methodology, the built-in variational analysis features in commercial behavioral simulators become important tools to evaluate manufacturability of MEMS designs.

Acknowledgement

The authors thank former students Jan Vandemeer and Michael Kranz for work on MEMS behavioral simulation and model generation. The research effort is sponsored by the Defense Advanced Research Projects Agency under the Air Force Research Laboratory, Air Force Materiel Command, USAF, under grant number F30602-96-2-0304 and in part by G.K.Fedder's National Science Foundation CAREER Award MIP-9625471.

References

[1] J.M. Karam, B. Courtois, K. Hofmann, A. Poppe, M. Rencz, M. Glesner, V. Szekely, "Micro-systems Modeling at a System Level", *APCHDL '96,* Bangalore, India, 8-10 January, 1996.

[2] *MEMCAD Web Page,* http://www.memcad.com, Microcosm Technologies, Inc., 201 Willesden Dr., Cary, NC 27513.

[3] *Intellisense Web Page,* http://www.intellis.com, IntelliSense Corporation, 16 Upton Dr., Wilmington, MA 01887.

[4] J. M. Funk, J. G. Korvink, J. Bühler, M. Båchtold, and H. Baltes, "SOLIDIS: A Tool for Microactuator Simulation in 3-D," *J. of Microelectromech. Sys.*, v. 6, no. 1, pp. 70-82, March 1997. (*SOLIDIS Web Page,* http://www.ise.ch/solidis)

[5] L. D. Gabbay and S. D. Senturia, "Automatic Generation of Dynamic Macro-Models using Quasistatic Simulations in Combination with Modal Analysis," *1998 Solid-State Sensors and Actuators Workshop,* Hilton Head Is., SC, June 7-11, 1998, pp. 197-200.

[6] J. Vandemeer, M.S. Kranz, and G. K. Fedder, "Hierarchical Representation and Simulation of Micromachined Inertial Sensors," *1998 Int. Conf. on Modeling and Simulation of Microsystems, Semiconductors, Sensors and Actuators (MSM '98),* Santa Clara, CA, April 6-8, 1998.

[7] I. Getreu, "Behavioral Modelling of Analog Blocks using the SABER Simulator,", Proc. Microwave Circuits and Systems, pp 977-980, August 1989.

[8] J. Clark, N. Zhou, S. Brown and K.S.J. Pister, "Nodal Analysis for MEMS Simulation and Design", *1998 Int. Conf. on Modeling and Simulation of Microsystems, Semiconductors, Sensors and Actuators (MSM '98),* Santa Clara, CA, April 6-8, 1998.

[9] J. V. Clark, N. Zhou, S. Brown and K.S.J. Pister, “MEMS Simulation Using SUGAR v0.5”, *1998 Solid-State Sensors and Actuators Workshop,* Hilton Head Is., SC, June 7-11, 1998, pp.191-196.

[10] G. Lorenz and R. Neul, “Network-Type Modeling of Micromachined Sensor Systems,” *1998 Int. Conf. on Modeling and Simulation of Microsystems, Semiconductors, Sensors and Actuators (MSM ‘98),* Santa Clara, CA, April 6-8, 1998.

[11] D. Teegarden, G. Lorenz and R. Neul, “How to Model and Simulate Microgyroscope Systems,” *IEEE Spectrum*, pp. 67-75, July 1998.

[12] *ADXL50 Accelerometer Data Sheet,* Analog Devices, Inc., One Technology Way, P.O.Box 9106, Norwood, MA 02062-9106, 1996 (http://www.analog.com).

[13] *MMAS40G10D Accelerometer Data Sheet,* Motorola Sensor Products, 1996 (http://design-net.com/senseon).

[14] M. A. Mignardi, “Digital Micromirror Array for Projection TV,” *Solid State Technology,* v.37, no.7, pp. 63-4, July 1994.

[15] D. A. Koester, R. Mahadevan, K. W. Markus, *Multi-User MEMS Processes (MUMPs) Introduction and Design Rules*, available from MCNC MEMS Technology Applications Center, 3021 Cornwallis Road, Research Triangle Park, NC 27709, rev. 3, Oct. 1994, 39 pages.

[16] W. C. Tang, T.-C. H. Nguyen, M. W. Judy, and R. T. Howe, “Electrostatic comb drive of lateral polysilicon resonators,” *Sensors and Actuators A*, vol.21, no.1-3, pp. 328-31, Feb. 1990.

[17] K. Wang and C. T.-C. Nguyen, “High-Order Micromechanical Electronic Filters,” *IEEE MEMS Workshop,* Nagoya, Japan, January 26-30, 1997, pp. 25-30.

[18] M. J. Daneman, N. C. Tien, O. Solgaard, K. Y. Lau, and R. S. Muller, “Linear Vibromotor-Actuated Micromachined microreflector for Integrated Optical Systems, *1996 Solid-State Sensors and Actuators Workshop,* Hilton Head Is., SC, June 2-6, 1996, pp. 109-112.

[19] J. Vandemeer, M.S. Kranz, and G. K. Fedder, “Nodal Simulation of Suspended MEMS with Multiple Degrees of Freedom,” *1997 Int. Mechanical Engineering Congress and Exposition: The Winter Annual Meeting of ASME in the 8th Symposium on Microelectromechanical Systems (DSC-Vol.62)*, Dallas, TX, 16-21 November, 1997, pp. 113-118.

[20] http://www.ece.cmu.edu/~mems/nodas.html

[21] S. P. Przemieniecki, *Theory of Matrix Structural Analysis,* McGraw-Hill, New York, New York, 1968.

[22] X. Zhang and W. C. Tang, “Viscous Air Damping in Laterally Driven Microresonators,” *Sensors and Materials,* v. 7, no. 6, pp.415-430, 1995.

[23] *ABAQUS Web Page,* http://www.hks.com, Hibbitt, Karlsson, and Sorensen, Inc., 1080 Main Street, Pawtucket, RI 02860.